

Miniaturized High-Performance Filters for 5G Small-Cell Applications

Muhammad Ali, Fuhan Liu, Atom Watanabe, P. Markondeya Raj,
Venkatesh Sundaram, Manos M. Tentzeris and Rao. R. Tummala
3D System Packaging Research Center
Georgia Institute of Technology
Atlanta, GA, USA
Email: ali_cmi@gatech.edu

Abstract—This paper demonstrates the first panel-based ultra-miniaturized filters with footprint smaller than half of the free-space wavelength at the operating frequencies of 28 and 39 GHz bands for 5G and mm-wave small-cell applications. The thin-film filters can be utilized either as ultra-thin integrated passive devices (IPDs) or embedded into the module substrates. Two filter types: lowpass and bandpass, with three topologies in total, are modeled, designed and fabricated on precision thin-film build-up layers on glass and traditional laminate cores. The modeling, design and optimization phase included the considerations of fabrication tolerances and testability of the filters. Glass is an ideal core material for mm-wave 5G modules and IPDs since it combines the benefits of ceramics for high frequency electrical performance, laminates for large panel processing and low cost, silicon-like dimensional stability and precision patterning, which is essential for mm-wave circuits. Unlike printing used in ceramics, or subtractive etching used in multilayer organics (MLO), this research utilizes semi-additive patterning (SAP) process to form high precision, multilayer redistribution layers (RDL) to design ultra-compact filter topologies with low insertion loss and improved stopband rejection, due to the close-to-ideal translation of lumped-to-distributed components. The simulated results of bandwidth, in-band insertion loss and out-of-band rejection of filters show excellent correlation with the measured results.

Index Terms—5G and mm-wave; small-cell; RF; filter; quasi-lumped; interdigital; hairpin; semi-additive process

I. INTRODUCTION

Wireless communication systems have been key enablers for the ubiquity of smart-phones and advancements in these systems will play a prominent role in realizing the true form of internet of things (IoT), automotive electronics for vehicle-to-vehicle (V2V) and vehicle-to-everything (V2X) connectivity for self-driving cars and seamless communication using a variety of communication standards for a range of applications. These have driven major breakthroughs in electronics and packaging innovation for multi-band multi-standard (MBMS) communications with GSM, WLAN, Bluetooth, 4G and LTE, GPS and mm-wave. All these technologies coexist in a single system. Miniaturized individual components and modules with increased functional density, maximum electromagnetic isolation and reduced footprint are essential to meet the growing demand for smart communication devices and systems for 5G networks, especially for mm-wave band infrastructure such as small-cells. [1], [2].

5G wireless systems will use mm-wave frequencies as a means to provide blazing fast data-rate of 100 Mbps to the end-users in metropolitan areas. The current limitation with 4G and LTE networks is the total usable fractional bandwidth (FBW). The same FBW at mm-wave frequencies provides much higher bandwidth, and thus, ability to provide the end-user with higher data-rates. This translates to increased complexity of electronics, which in turn, drives platform integration. The ongoing challenge of MBMS RF solutions for smartphones, essentially carrier aggregation (CA), requires the addition of more bands within the same physical space of user-equipment (UE) [3]. The requirement to use mm-waves for communications leads to complex filtering challenges such as low in-band insertion loss and high out-of-band rejection: a daunting task beyond 20 GHz. Small-cell front-end modules (FEMs) will also deploy advanced filtering technologies to isolate the communication bands from nearby interferers [4]. To address this issue, designers have resorted to either connecting stand-alone filters to one antenna accessed by a switch, often called a CA switch, or they resort to using multiplexers with very high Q filters [5], [6].

A typical architecture of a front-end module with integrated duplexer (FEMiD) is shown in Fig. 1, which depicts a number of bandpass filters in the duplexer. These filters correspond to band filters for 4G and LTE systems. Standalone filters are used in chip-to-antenna interconnections before the amplifier

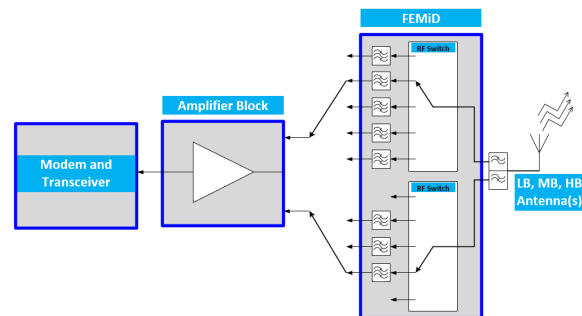


Figure 1. A generic architecture of FEMiD

block in a front-end to isolate the band of interest and improve noise figure of the overall system. Current limitation on number of CA bands is 5. However, 4G+ or advanced 4G will have over 49 combinations of LTE bands and this limit is altogether terminated from 5G systems [7]. Increasing CA bands translates to more band filters, which can be approximately 100 in small-cell and UE. Total number of CA bands under sub-6 GHz, including mm-wave bands, is projected to be 30-40 for local multi-point distribution service (LMDS) and UE by 2020 [8]. This puts immense pressure on filter design and ramps up its design and fabrication complexity as multiple-input multiple-output (MIMO) systems expand with increasing consumer demands. Traditionally, mm-wave components are designed on chip as they require very tight process control. However, off-chip implementation of these filters on package-level is enabled by high-precision RDL on materials such as glass with on-chip like tolerances, which can result in low loss, compact and high-Q filter structures due to better materials.

Similarly, mm-wave front-ends on infrastructure side, specifically in small-cells for short-range communication, require advancements in component design in terms of low cost, high performance and reliability. Sub-6 GHz communication filtering is dominated by acoustic wave technologies such as SAW and BAW filters [9]. However, these technologies do not scale to mm-wave frequencies and a new approach is required to design and fabricate high-performance filters for mm-wave bands of 5G communication systems. In addition to delivering higher performance, form-factor also governs the use of a particular filter in a specific application. Meeting the requirements of wide bandwidth, sharp-rejection and compact size is often subjected to certain trade-offs. For techniques involving coupled lines, the fabrication becomes challenging for wide bandwidth requirements [10].

This paper demonstrates filters with footprint smaller than half of the free-space wavelength at the operating frequency of 28 (24.5-29.5 GHz, FBW=18.51%) and 39 GHz (37.0-43.5 GHz, FBW=16.15%) bands for 5G applications by utilizing precision low-loss RDL for highly-integrated mixed-signal systems. Two filter types: lowpass (LPF) and bandpass (BPF), with three topologies in total, are modeled, designed and fabricated inside thin-film build-up layers on glass and traditional laminate cores. Utilizing glass core combines the benefits of ceramic or low-loss polymers for electrical performance, and silicon-like dimensional stability of glass for precision panel-scale patterning. Multilayered RDL with sub-40 micron features are utilized to design innovative filter topologies with benefits in stopband rejection due to close-to-ideal modeling of inductive distributed transmission lines [11].

This paper is organized as follows: An introduction to the motivation and applications of this research is given in Section-1. The materials stackup and design techniques for the demonstration of LPFs and BPFs is discussed in Section-2 followed by the detail of fabrication process in the Section-3. Finally, a comparison of simulated and measured results is given in Section-4.

II. MATERIAL STACKUP, MODELING AND DESIGN PROCEDURE OF FILTERS

In this section, the material stackup and design procedure of filters is discussed. The filters can be designed as IPDs or embedded into the module substrates. The material stackup is shown in Fig. 2. A ultra-thin core substrate, which can be either glass or laminate, is chosen for this demonstration. Glass-based packages are emerging as an ideal candidate to realize mm-wave technologies because of its superior dimensional stability, availability in large-area low-cost panels, ability to form fine-pitch through-vias, stability to temperature and humidity, and matched coefficient of thermal expansion (CTE) with devices along with low dielectric loss compared to silicon and mold compounds used in fan-out packages [12]. For discrete components, the core only serves as a carrier. Therefore, in applications where these filters are to be used as IPDs, glass is suggested as the choice of core material since its CTE can be matched to other materials. Glass and low loss laminate cores with thickness of 100-150 μm were chosen for this study.

A 72.5 μm -thick epoxy film from Aginomoto (ABF GL102) is chosen as the buildup dielectric for the filter structures. It has the following electrical properties : dielectric constant (Dk) = 3.3 and loss tangent (Df): 0.0044 at 5.8 GHz. The desired copper thickness for the microstrip filter structures is targeted to be 8 μm . The skin-depth at the highest frequency



Figure 2. Material stackup for demonstration of filters

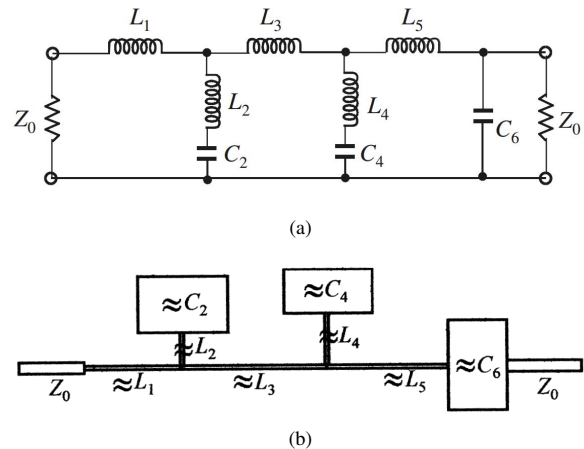


Figure 3. An elliptic lowpass filter (a) lumped-element prototype, and (b) microstrip realization of the elliptic function lowpass filter

of 43.5 GHz is approximately $0.32 \mu\text{m}$, which gives enough room to conveniently fabricate the microstrip transmission lines with decent power handling capabilities while keeping the conductor thickness more than five times of skin-depth for low-loss applications. Finally, the blind-via diameter is chosen to be at the industry standard of $60 \mu\text{m}$, which gives an aspect ratio (substrate thickness/via diameter) of 1.2 for plating. The minimum center-to-center via pitch is twice the via diameter or $120 \mu\text{m}$. This material stackup is used in simulation using Keysight Advanced Design System (ADS) for all the filters in this demonstration.

A. Lowpass Filter Design

The structures chosen for lowpass filter are elliptical/semi-lumped with finite-frequency infinite-attenuation poles [13]. Elliptic transfer functions have a ripple in both pass- and stopband but they provide the steepest roll-off as compared to maximally flat and Chebyshev transfer functions. A lumped-element lowpass prototype of elliptical LPFs is shown in Fig. 3a along with its microstrip realization in Fig. 3b. The procedure to design this lowpass filter structure, given in detail in [13], is summarized below:

- 1) Find filter order (N) based off desired attenuation in stopband.
- 2) Select g-values for the desired order. g-values are unity-impedance unity-frequency values for a lowpass filter prototype.
- 3) Scale g-values to the desired impedance and frequency to find L & C values using (1).

$$\begin{aligned} L_i &= \frac{1}{2\pi f_c} Z_0 g_{Li} \\ C_i &= \frac{1}{2\pi f_c} \frac{1}{Z_0} g_{Ci} \end{aligned} \quad (1)$$

where, f_c =cut-off frequency of lowpass filter, Z_0 =characteristic impedance (usually 50Ω), g_{Li} =g-values of the filter corresponding to inductors, g_{Ci} =g-values of the filter corresponding to capacitors

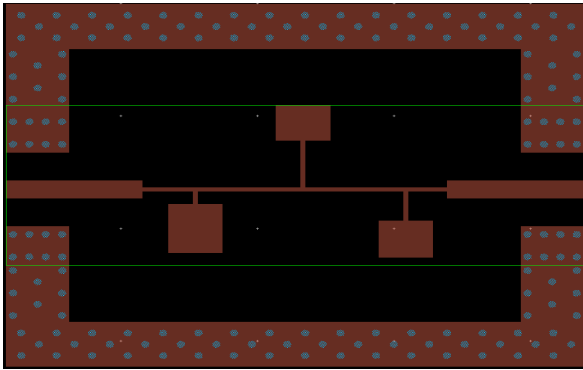


Figure 4. Layout of a 7th order LPF for 28 GHz band

TABLE I. DESIGN PARAMETERS OF A 7TH ORDER LPF FOR 28 GHz BAND

Parameter	Value
Cut-off Frequency	29.5 GHz
Insertion loss at cut-off frequency	<2 dB
30-dB attenuation point to band-edge ratio	<1.24
Highest impedance (Inductor)	100.53 Ω
Smallest line width (Inductor)	35.90 μm
Lowest impedance (Capacitor)	27.20 Ω
Largest line width (Capacitor)	399.80 μm
Filter dimensions (Physical)	$4.23 \times 1.42 \text{ mm}^2$

- 4) Equation (2) can be used to find the physical length corresponding to each lumped L & C for microstrip structure.

$$\begin{aligned} l_{Li} &= \frac{\lambda_{gL}(f_c)}{2\pi} \arcsin(2\pi f_c \frac{L_i}{Z_{0L}}) \\ l_{Ci} &= \frac{\lambda_{gC}(f_c)}{2\pi} \arcsin(2\pi f_c Z_{0C} C_i) \end{aligned} \quad (2)$$

where, $\lambda_{gL}(f_c)$ and $\lambda_{gC}(f_c)$ are guide wavelengths corresponding to L and C at the cut-off frequency, Z_{0L} =characteristic impedance of the inductor ($> Z_0$), Z_{0C} =characteristic impedance of the capacitor ($< Z_0$), Z_{0L} & Z_{0C} are the choice of designer as they physically correspond to the width of transmission lines (microstrip) to be fabricated. In this demonstration, the impedances are set to obtain the smallest line width of $26.4 \mu\text{m}$.

- 5) Apply required compensations for the unwanted reactance/susceptance at the junction of the inductive line elements shown in Fig. 3(b).
- 6) Simulate and optimize in ADS Schematic and Momentum.
- 7) Finalize layout: Add ground pads (GSG) for testing, connect GSG ground planes through a rectangular path and make a boundary to define filter size.

Using this method, a 7th order LPF for 28 GHz band with cut-off frequency (f_c) of 29.5 GHz is modeled, simulated and optimized in the frequency range of DC-50 GHz. The layout of a 7th order LPF for 28 GHz band is shown in Fig. 4 with important design parameters given in Table I.

B. Bandpass Filter Design

For the bandpass filters, interdigital and hairpin structures are chosen for 28 and 39 GHz bands, respectively. Hairpin bandpass filters use parallel-coupled half-wavelength ($\lambda/2$) open resonators, whereas interdigital filters use quarter-wavelength ($\lambda/4$) short resonators, making both these structures an ideal choice for small footprint [13], [14]. The design process of both these filters is given in detail in [14]. A relatively modern technique with explicit design equations is given in [15] for interdigital filters.

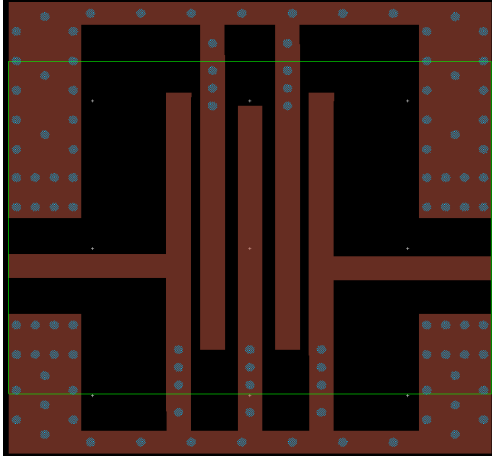


Figure 5. Layout of a 5th order interdigital BPF for 28 GHz band

TABLE II. DESIGN PARAMETERS OF A 5TH ORDER INTERDIGITAL BPF FOR 28 GHz BAND

Parameter	Value
Cut-off frequencies	24.5 and 29.5 GHz
Insertion loss at cut-off frequencies	<2.5 dB
30-dB attenuation point to band-edge ratio	<1.20
Resonator width	156.91 μm
Filter dimensions (Physical)	3.06 \times 2.25 mm ²

It is to be noted that the resonators for interdigital filters have fixed width and the spacing between resonators is adjusted to obtain the desired response. Both interdigital and hairpin filters are designed using Chebyshev polynomial g -values. Using this method, the following BPFs are modeled, simulated and optimized in the frequency range of 14-50 GHz:

- 28 GHz band ($f_c=24.5$ and 29.5 GHz): 5th order Interdigital BPF
- 39 GHz band ($f_c=37.0$ and 43.5 GHz): 5th order Hairpin BPF

The layout of a 5th order interdigital filter for 28 GHz band

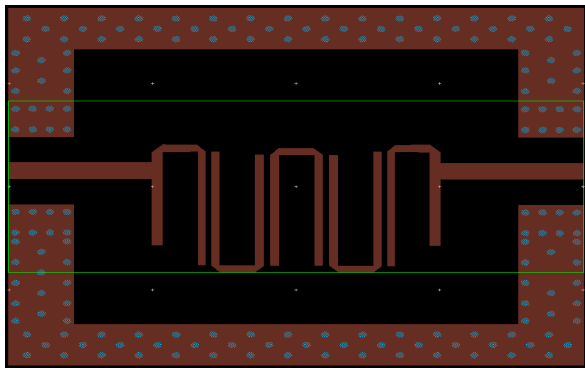


Figure 6. Layout of a 5th order hairpin BPF for 39 GHz band

TABLE III. DESIGN PARAMETERS OF A 5TH ORDER HAIRPIN BPF FOR 39 GHz BAND

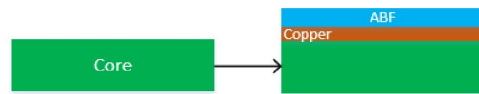
Parameter	Value
Cut-off Frequencies	37.0 and 43.5 GHz
Insertion loss at cut-off frequencies	<2 dB
30-dB attenuation point to band-edge ratio	<1.20
Resonator Width	61.71 μm
Filter Dimensions (Physical)	3.85 \times 1.66 mm ²

is shown in Fig. 5, with important design parameters given in Table II. Similarly, the layout of a 5th order hairpin filter for 39 GHz band is shown in Fig. 6, with important design parameters given in Table III.

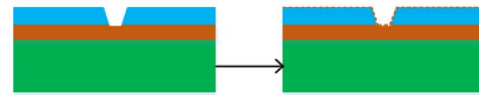
III. FABRICATION PROCESS OF FILTERS

The fabrication process uses the semi-additive patterning (SAP) process to pattern polymers. SAP is illustrated with

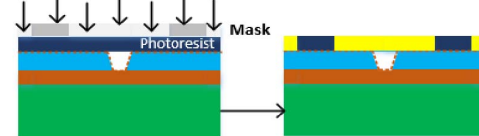
Copper Deposition and ABF Lamination



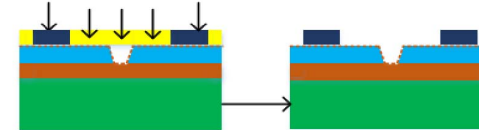
Laser Via Ablation and Seed Layer Deposition



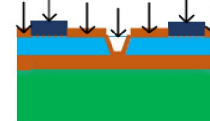
UV Exposure



PR Development



Electrolytic Cu Plating



Photoresist Stripping and Seed Layer Etching

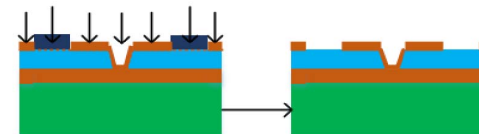


Figure 7. Illustration of SAP with step-by-step cross-sections

cross-sections in each step in Fig. 7.

The process starts with a copper-clad core substrate whose surface is treated using Novabond wet process by Atotech to enhance the adhesion strength of the ABF film that is bonded onto the substrate [16]. Novabond improves the adhesion of copper to ABF both chemically and mechanically by forming nano-anchor structures to lock the polymer film. After lamination and curing of ABF GL102 dry-film using a vacuum laminator, blind vias are drilled using a UV laser. The via ablation conditions are optimized in terms of power, power density and number of repetitions, to avoid any damage to the copper underneath the film while ensuring desired via depth. On the laminated polymer, a copper seed layer with a thickness of $0.2 \mu\text{m}$ is uniformly deposited. Adhesion of electroless copper to polymer is improved by prior roughening of the polymer surface using a permanganate chemical etch to create mechanical anchor sites. The wet chemical etch also removes the residual polymer on copper surfaces after via ablation.

The top and bottom layers are laminated with a $15 \mu\text{m}$ dry-film negative photoresist and patterned using a mylar mask on a photolithography tool. The exposure time needs to be optimized carefully to obtain dimensionally-accurate feature size. After photoresist development, the panel is subjected to O_2 plasma to remove photoresist residue and improve the wettability of electrolyte on copper. The metalization of traces is performed using electroplating. SAP on a dimensionally-stable core provides excellent dimensional control when a fine feature size is required, such as in this application, which helps in maintaining the rectangular profile of lines as opposed to convex profile achieved after subtractive etching procedures. Moreover, the dimensional control is the result of avoiding long etching intervals and lateral undercuts usually prevalent in subtractive etching. The authors strive to achieve $8.2 \mu\text{m}$ copper thickness considering that the removal of seed layer at the end of SAP leads to the targeted copper thickness of $8 \mu\text{m}$. The photoresist is removed using a stripper solvent, and seed layer etching is performed as the last step of this process. The measured copper thickness after fabrication process is $8.5 \pm 0.5 \mu\text{m}$. The fabrication process requires special handling procedures if ultra-thin glass is used a core substrate [17], [18].

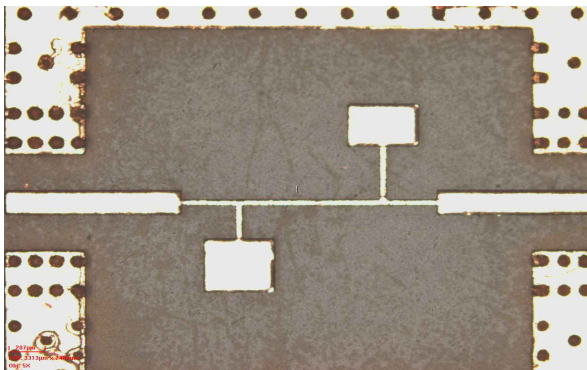
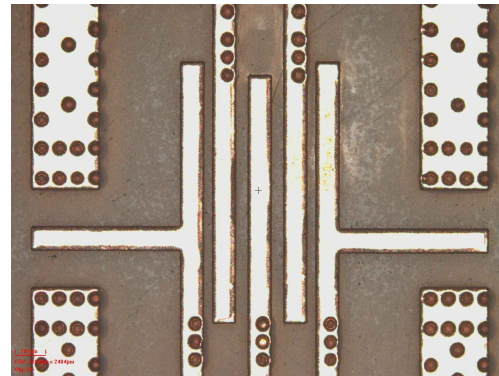
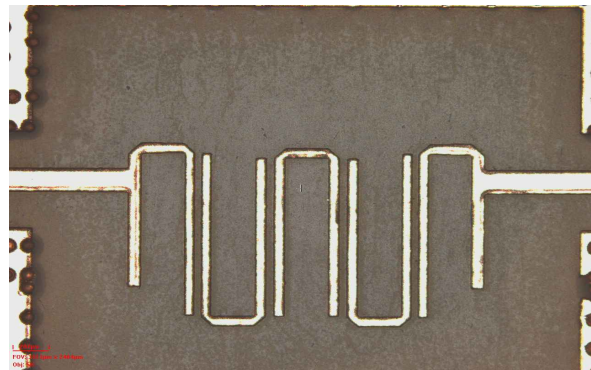


Figure 8. A fabricated 7th order LPF for 28 GHz band



(a)



(b)

Figure 9. Fabricated BPFs (a) 5th order interdigital for 28 GHz band, (b) 5th order hairpin for 39 GHz band

A fabricated 7th order LPF for 28 GHz band is shown in Fig. 8. Fabricated interdigital and hairpin bandpass filters are shown in Fig 9a and Fig. 9b, respectively.

IV. CHARACTERIZATION RESULTS AND ANALYSIS

In this section, the characterization results of fabricated filters are discussed in detail. The measurements are performed using Keysight E8361C PNA in the frequency range of 14-50 GHz using ACP50 GSG probes and Short-Open-Load-Through (SOLT) calibration. The measurement is performed on five coupons of each filter. The measurement results are compared with simulation results to perform a model-to-hardware correlation study. Moreover, dimensional analysis is performed to analyze the fabricated dimensions and compare them with the dimensions in simulation.

A. Lowpass Filters

The measurement results of fabricated LPF for 28 GHz band is shown in Fig. 10, along with their simulated results. Excellent model-to-hardware correlation is observed in all the fabricated filters, indicating the accuracy of fabrication process within a very strict tolerance factor. The measured response of this filter shows less than 2 dB insertion loss at f_c and 30-dB attenuation point to band-edge ratio less than 1.25, which matches the optimized ADS model. The filters also

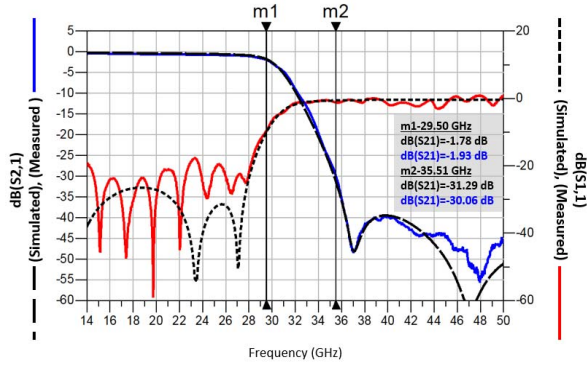


Figure 10. A fabricated 7th order LPF for 28 GHz band

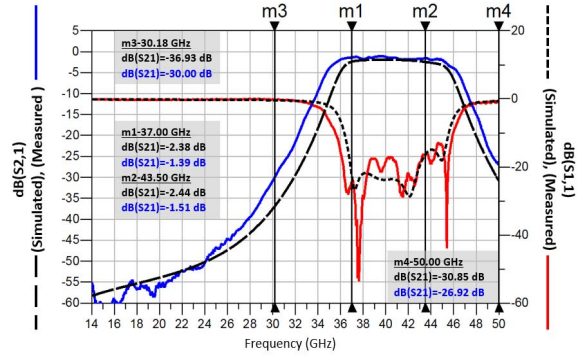


Figure 12. A fabricated 5th order hairpin BPF for 39 GHz band

show exceptional return loss: $\text{dB}(S(1,1))$ is below -20 dB which corresponds to a VSWR better than 1.22, indicating an outstanding impedance match.

B. Bandpass Filters

In this section, simulated and measured results of interdigital and hairpin bandpass filters are compared and analyzed based on their response.

1) *Interdigital Bandpass Filters*: For 28 GHz band, a 5th order interdigital BPFs is modeled, designed, optimized, fabricated and characterized. The simulated and measured results are compared in Fig. 11.

As evident in the Fig. 11, the filter exhibits more bandwidth than their simulated versions and are slightly shifted in frequency. This is attributed to the slight increase in resonator width during exposure in the photolithography step during fabrication. The dose time is optimized for small line-widths as indicated earlier. Due to this optimization, the wider resonator traces, such as in interdigital filters, are affected. The spacing between the resonators decreases, resulting in a slightly wider bandwidth. However, despite this effect, the fabricated interdigital BPF depicts a mid-band insertion loss of 2.6 dB, has 30-dB attenuation point to band-edge ratio of 1.16 and a VSWR better than 1.25.

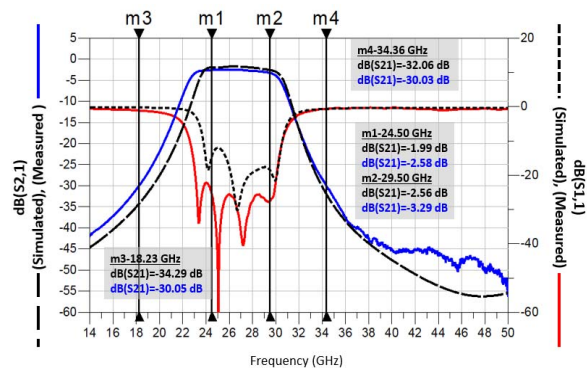


Figure 11. A fabricated 5th order interdigital BPF for 28 GHz band

2) *Hairpin Bandpass Filters*: A 5th order hairpin BPF for 39 GHz band is modeled, designed, optimized, fabricated and characterized. Similar to the interdigital bandpass filter, it has a slightly higher bandwidth but is not affected by frequency shift, as depicted in Fig 12. The fabricated hairpin BPF for 39 GHz band has a measured insertion loss of 1.43 dB, 30-dB attenuation point to band-edge ratio of 1.19 and has VSWR below 1.6.

C. Analysis

1) *Dimensional Analysis*: Dimensional analysis of all the fabricated filters is performed to find the discrepancy between the desired and obtained resonator widths and spacings. It also provides the physical measurements of filter size to translate it into electrical size. It was observed that the resonator widths for BPFs are affected by a nominal variation of $3\text{-}4\ \mu\text{m}$ whereas the variation in high impedance lines in fabricated LPFs is only $1\text{-}1.5\ \mu\text{m}$.

The physical dimensions along with the corresponding electrical dimensions in terms of λ_0 of each fabricated filter is given in Table IV. The physical dimensions of 28 GHz bandpass filter is normalized by corresponding free-space wavelength of 28 GHz: 10.71 mm and the physical dimensions of 39 GHz BPF are normalized by its corresponding free-space wavelength of 39 GHz: 7.69 mm. As evident from the electrical dimensions of the filters given in Table IV, all filters have footprint smaller than $0.5\lambda_0 \times 0.5\lambda_0$.

TABLE IV. PHYSICAL AND ELECTRICAL DIMENSIONS OF FABRICATED FILTERS

Filter	Physical Dimensions (mm ²)	Electrical Dimensions (λ_0) ²
7 th order LPF for 28 GHz band	4.23×1.42	0.39×0.13
5 th order Interdigital BPF for 28 GHz band	3.06×2.25	0.29×0.21
5 th order Hairpin BPF for 39 GHz band	3.85×1.66	0.50×0.22

TABLE V. COMPARISON WITH SIMILAR FILTERS

Reference Filter	Type	f_0 and FBW	Insertion Loss	Size (λ_0) ²
[19]	Dual-Mode Resonator on LTCC	30 GHz and 0.05%	2.95 dB	1.1×0.8
[20]	Vertically stacked SIW on LTCC	29.87 GHz and 13%	3.3 dB	0.37×0.28
[21]	Stacked SIW on LTCC	27.95 GHz and 3.7%	2.8 dB	0.57×0.30
[22]	High-Order mode SIW on PCB	35.8 GHz and 13%	3 dB	0.94×0.51
[23]	Coupled-line microstrip on Teflon	27.85 GHz and 0.05%	4 dB	0.43×0.23
[23]	Coupled-line microstrip on Alumina	38.5 GHz and 0.08%	3 dB	0.60×0.31
This work	Interdigital on ultra-thin laminated core	27 GHz and 18.51%	2.6 dB	0.29×0.21
This work	Hairpin on ultra-thin laminated core	40.25 GHz and 16.15%	1.43 dB	0.52×0.22

2) *Comparison with similar filters:* A performance comparison between this paper and other similar filter structures in literature is presented in Table V.

To the best knowledge of the authors, the fabricated filters are smallest in terms of x-y dimensions as well as z-height. The total height of the filters is 188.5 μm including the core thickness. Moreover, they depict superior performance in terms of in-band insertion loss, out-of-band rejection and impedance matching.

V. CONCLUSIONS

Miniaturized high-performance filters for 5G small-cell applications with footprint smaller than half of the free-space wavelength at the operating frequency of 28 and 39 GHz bands are demonstrated on ultra-thin build-up dielectrics on thin substrates. Two filter types with three topologies in total are modeled, designed, optimized, fabricated and characterized. The filters are fabricated using SAP process that is fine-tuned to meet the dimensional accuracy required by these filter structures. The characterization results showed excellent correlation with the simulated response for all the fabricated filters. The fabricated filters depicted low in-band insertion loss, high out-of-band rejection and very low VSWR, indicating an excellent impedance match. Small footprint of the filters, combined with their reduced height, makes them ideal for several 5G and mm-wave applications.

ACKNOWLEDGMENT

The authors wish to acknowledge the industry sponsors of the consortia program at GT-PRC for their technical guidance and support.

REFERENCES

- [1] R. Tummala, *System on Package: Miniaturization of the Entire System*, ser. McGraw Hill professional. McGraw-Hill Education, 2007. [Online]. Available: <http://bit.ly/2GUXBjX>
- [2] J. Q. Hardik Gandhi, Debbi Greenstreet, "Digital radio front-end strategies provide game-changing benefits for small cell," <http://bit.ly/2HWceoD>, Texas Instruments, 2013.
- [3] G. G. Fattering, A. Volatier, M. Al-Joumayly, Y. Yusuf, R. Aigner, N. Khlaf, and M. Granger-Jones, "Carrier aggregation and its challenges: The golden age for acoustic filters," in *2016 IEEE MTT-S International Microwave Symposium (IMS)*, May 2016, pp. 1–4.
- [4] S. Mahon, "The 5g effect on rf filter technologies," *IEEE Transactions on Semiconductor Manufacturing*, vol. 30, no. 4, pp. 494–499, Nov 2017.
- [5] "Addressing carrier aggregation challenges using multiplexer solutions," <http://bit.ly/2GW6Al8>, Qorvo, January 2016.
- [6] N. Athanasopoulos, D. Makris, and K. Voudouris, "Development of a 60 ghz substrate integrated waveguide planar diplexer," in *2011 IEEE MTT-S International Microwave Workshop Series on Millimeter Wave Integration Technologies*, Sept 2011, pp. 128–131.
- [7] I. Poole, "What is lte carrier aggregation," <http://bit.ly/2FbTTFf>, Radio-Electronics.com.
- [8] J. Madden, "Industry voices—madden: Who holds the 5g spectrum in major u.s. cities?" <http://bit.ly/2CTUTZx>, Mobile Experts LLC.
- [9] R. Aigner, "Saw and baw technologies for rf filter applications: A review of the relative strengths and weaknesses," in *2008 IEEE Ultrasonics Symposium*, Nov 2008, pp. 582–589.
- [10] M. Ali and T. Abbas, "Compact, meandered-line microstrip bandpass filter," in *Multi-Topic Conference (INMIC), 2014 IEEE 17th International*. IEEE, 2014, pp. 67–72.
- [11] V. Sukumaran, Q. Chen, F. Liu, N. Kumbhat, T. Bandyopadhyay, H. Chan, S. Min, C. Nopper, V. Sundaram, and R. Tummala, "Through-package-via formation and metallization of glass interposers," in *Electronic Components and Technology Conference (ECTC), 2010 Proceedings 60th*. IEEE, 2010, pp. 557–563.
- [12] J. Tong, V. Sundaram, A. Shorey, and R. Tummala, "Substrate-integrated waveguides in glass interposers with through-package-vias," in *Electronic Components and Technology Conference (ECTC), 2015 IEEE 65th*. IEEE, 2015, pp. 2222–2227.
- [13] J.-S. G. Hong and M. J. Lancaster, *Microstrip filters for RF/microwave applications*. John Wiley & Sons, 2004, vol. 167.
- [14] G. Matthaei, L. Young, and E. Jones, "Design of microwave filters, impedance-matching networks, and coupling structures," Stanford Research Inst Menlo Park CA, Tech. Rep., 1963.
- [15] S. Caspi and J. Adelman, "Design of combline and interdigital filters with tapped-line input," *IEEE Transactions on Microwave Theory and Techniques*, vol. 36, no. 4, pp. 759–763, Apr 1988.
- [16] "Novabond-it," <http://bit.ly/2FKHw13>, Atotech.
- [17] H. Lu, R. Furuya, B. M. D. Sawyer, C. Nair, F. Liu, V. Sundaram, and R. R. Tummala, "Design, modeling, fabrication and characterization of 2-5 micron redistribution layer traces by advanced semiadditive processes on low-cost panel-based glass interposers," *IEEE Transactions on Components, Packaging and Manufacturing Technology*, vol. 6, no. 6, pp. 959–967, June 2016.
- [18] A. O. Watanabe, M. Ali, B. Tehrani, J. Hester, H. Matsuura, T. Ogawa, P. M. Raj, V. Sundaram, M. M. Tentzeris, and R. R. Tummala, "First demonstration of 28 ghz and 39 ghz transmission lines and antennas on glass substrates for 5g modules," in *2017 IEEE 67th Electronic Components and Technology Conference (ECTC)*, May 2017, pp. 236–241.
- [19] K. Ahn and I. Yom, "A ka-band multilayer ltcc 4-pole bandpass filter using dual-mode cavity resonators," in *2008 IEEE MTT-S International Microwave Symposium Digest*, June 2008, pp. 1235–1238.
- [20] T. M. Shen, T. Y. Lin, T. Y. Huang, and R. B. Wu, "A vertically stacked quasi-elliptic waveguide filter with crossly coupling vias," in *2007 Asia-Pacific Microwave Conference*, Dec 2007, pp. 1–4.

- [21] K. S. Chin, C. C. Chang, C. H. Chen, Z. Guo, D. Wang, and W. Che, "Ltc multilayered substrate-integrated waveguide filter with enhanced frequency selectivity for system-in-package applications," *IEEE Transactions on Components, Packaging and Manufacturing Technology*, vol. 4, no. 4, pp. 664–672, April 2014.
- [22] Y. Tao, W. Hong, and H. Tang, "Design of a ka-band bandpass filter based on high order mode siw resonator," in *2006 7th International Symposium on Antennas, Propagation EM Theory*, Oct 2006, pp. 1–3.
- [23] Y. M. Yan, Y. T. Chang, H. Wang, R. B. Wu, and C. H. Chen, "Highly selective microstrip bandpass filters in ka-band," in *2002 32nd European Microwave Conference*, Sept 2002, pp. 1–4.